Application Of Nnw-Flowstar Software in Transport Aircraft Simulation

Peihong Zhang, Anlin Jiang, Yaobing Zhang, Wei Xiao, Wei Zhao *, Xiaojun Wu

Computational Aerodynamic Institute of China Aerodynamic Research & Development Center, Mianyang, China

*Corresponding author e-mail: ethnuaa@163.com

Abstract. Transport configuration usually use multi-segment swept wing with medium or high aspect ratio. Its flow includes wake flow, boundary layer interference, separated flow, wingtip vortex, transition and other complex flow phenomena, which poses a serious challenge on numerical simulation. Based on the self-developed National Numerical Wind Tunnel Project software named NNW-FlowStar and using unstructured hybrid grid technology, the validation research of simulation of transport aircraft is carried out. The NASA common research model (CRM) is the standard model of the 6th AIAA CFD drag prediction workshop. The effects of grid convergence, different turbulence models and quadratic constitutive relation correction are performed. The prediction accuracy of drag increment due to nacelle and pylon is analyzed. The results show that a nearly linear convergence property is achieved with grid refinement and the numerical method in this paper has second-order accuracy. The predicted results of drag at constant lift obtained by different turbulence models and drag increment due to nacelle and pylon agree well with the experimental data. The results obtained using SST turbulence model and quadratic constitutive relation correction are in good agreement with the experimental data. The reliability and effectiveness of the SST turbulence model and quadratic constitutive relation correction method for simulating the flow of transport configuration are validated.

Keywords: Nnw-Flowstar, Transport aircraft, simulation.

1. Introduction

With the development of numerical simulation technologies such as grid generation technology, flow field solving, and high-performance computers, CFD based on the Navier-Stokes equation is playing an increasingly important role in the aerospace field, and is widely used in the simulation of various aircraft aerodynamic characteristics and complex flow fields [1]-[4]. Commercial and military transport aircraft usually employ moderate or high-aspect-ratio swept wings, and the flow around the wing often involves complex flow phenomena such as wake, boundary layer interaction, flow separation, wingtip vortex, laminar flow, and transition, which pose severe challenges to CFD simulation methods and grid generation techniques [5]. The credibility of using RANS equations to simulate aerodynamic characteristics such as drag coefficient, maximum lift coefficient, and stall angle of attack for transport-class aircraft needs to be further improved, and accurately predicting flow separation in the flow field still faces great difficulties [6].

In order to evaluate the accuracy of CFD technology in simulating the drag prediction of transport aircraft, verify the simulation capabilities of CFD for transport aircraft, and provide advice and suggestions for the development of CFD technology, AIAA hosted the first drag prediction conference[7], DPW I (the 1st Drag Prediction Workshop), in June 2001. By stipulating standard calculation methods for aerodynamic forces and moments of transport aircraft transonic flow fields, providing standard grids, encouraging the generation of self-generated grids, stipulating standard calculation conditions, and providing corresponding experimental results, universities, research institutes, and industrial departments around the world are invited to jointly evaluate the current level of development of CFD methods for predicting aerodynamic forces and moments of transport aircraft transonic flow fields. An open and fair platform is provided to evaluate the effectiveness of existing

CFD codes and simulation techniques, and identify the direction of research and development that needs to be strengthened for CFD simulation, thus promoting the improvement of CFD application level. The AIAA DPW conference has been held for six times since June 2001 [8]. During the meeting, the reliability of aerodynamic force and moment prediction for the standard model was discussed in depth.

The standard computational configuration for the first DPW conference [7] was the DLR-F4 wing-body combination, with a focus on drag and polar curve prediction under fixed lift coefficients. The standard computational configurations for the second DPW conference [9] are the DLR-F6 wing-body combination and the DLR-F6 wing/body/frame/cabin configurations, with a focus on grid convergence and polar curve prediction under fixed lift coefficients, while evaluating the ability of CFD technology to simulate the installation resistance of pylons and nacelles. The standard computational configurations for the third DPW conference [10] were the DLR-F6 wing-body combination and the DLR-F6-FX2B wing-body combination. In order to encourage more software and researchers to participate, two separate wing configurations, DPW-W1 and DPW-W2, were added, focusing on grid convergence and polar curve prediction under fixed lift coefficients, while evaluating the ability of CFD technology to simulate the impact of local modifications on aerodynamic characteristics. For the first time, the "blind test" method was used, in which the test results were not announced in advance. The fourth to sixth DPW conferences [8] adopted the Boeing-redesigned CRM (Common Research Model) configuration as the standard computational shape, focusing on grid convergence, prediction of the impact of mounting resistance on pylons/nacelles, wing downwash flow, Mach number, Reynolds number, and static aero elastic effects.

Based on the software simulation results submitted at previous DPW conferences, it can be seen that the unstructured grid technology is the trend and direction of the future development of CFD simulation. A total of 17 research institutions at the 4th DPW Conference [11] used 16 software packages to provide 28 sets of numerical simulation results, including 17 sets using unstructured grid technology and 11 sets using structured grid technology, with the use of unstructured grid technology accounting for 60.7%. A total of 22 research institutions at the fifth DPW conference [12] used 11 software packages to provide 54 sets of numerical simulation results, including 26 sets using unstructured grid technology and 12 sets using structured grid technology. In addition, 16 sets used self-generated grids, including 8 sets using unstructured grid technology, accounting for 63.0% of the total. A total of 25 research institutions used 25 software packages to provide 48 sets of numerical simulation results at the 6th DPW conference [5]. Of these, 32 sets used unstructured grid technology, 9 sets used structured grid technology, and 5 sets used Cartesian grid technology. The proportion of unstructured grid technology was 66.7%.

In recent years, some Chinese scholars have also carried out research on the validation and confirmation of benchmark models. DENG X. G., ZONG W. G. [13] have analyzed the development of CFD validation and confirmation, and have put forward many constructive suggestions and opinions on the credibility evaluation of CFD software. CHEN S. S., LIU L. Y., YAN C., et al. [14] have developed an automated cloud platform for CFD software verification and validation. The China Aerodynamics Research and Development Center independently designed the transport aircraft standard model CHN-T1 [15], conducted a series of highly reliable wind tunnel tests in multiple wind tunnels, and organized the first aviation CFD credibility workshop in April 2018 to promote the development of domestic CFD verification and validation work. Starting from 2018, with the support of the National Numerical Wind Tunnel Engineering Project, the project team, in collaboration with domestic leading institutions, established a database of benchmark models dedicated to CFD verification and validation, and used these benchmark data to carry out a series of verification and validation work for aeronautical CFD [16].

Based on the self-developed NNW-FlowStar software [17][18] for the National Numerical Wind Tunnel Project and the unstructured hybrid grid technology, this article conducts numerical simulation research on the sixth DPW Computational Shape CRM, with the main aim of evaluating the ability of the NNW-FlowStar software to simulate transport aircraft and verifying the credibility of the software's simulation of transport aircraft. The discrete accuracy of the numerical method was analyzed through grid convergence studies. The predicted results of the CRM drag force and drag increment with different turbulence models and the addition of pylon and pod were compared with experimental values, verifying the reliability of the SST turbulence model with QCR correction method for simulating the flow of transport aircraft.

2. Numerical simulation method

NNW-FlowStar software is a large-scale general-purpose CFD computational analysis software developed independently by the project team with the support of the National Numerical Wind Tunnel Project, based on unstructured hybrid grids and MPI parallel technology. The software focuses on aerodynamic analysis of aircraft in the aerospace field, featuring efficient, robust, and accurate steady/unsteady numerical simulation, with characteristics of multi-body separation such as separation and staging. The goal of the software is to serve the fluid analysis and design of the national aerospace industry. The core solver has undergone extensive testing with benchmark data and complex engineering shapes, and was released nationwide for free in September 2020.

The flow control equation is the unsteady N-S equation, and the finite volume method is used to discretize the control equation. The unknown variables are stored in the body center of the grid cell:

$$\frac{\partial}{\partial t}\int_{\Omega}\vec{W}d\Omega+\oiint_{\partial\Omega}(\vec{F}_c-\vec{F}_v)dS=0 \tag{1}$$

In the equation, Ω represents the volume of the control volume, $\partial\Omega$ represents the area of the closed surface of the control volume, $\vec{W}$ is the conserved variable, $\vec{F}_c$ is the inviscid flux, and $\vec{F}_v$ is the viscous flux.

The Roe flux difference splitting method is used to discretize the flow rate, which has high discontinuity and viscosity resolution. The use of linear reconstruction within the unit enables second-order accuracy in spatial discretization, while the Venkatakrishnan limiter is used to suppress oscillations near discontinuities. Variable gradient solving uses a node-based Gauss method. The viscous flux is discretized using central difference. The first-order Euler backward difference with the local time step is used to achieve steady state. The Jacobian flux is obtained using a first-order upwind scheme, and the LU-SGS method is used to solve the discrete equations. Multi-grid is used to accelerate convergence.

The calculation assumes that the flow field is fully turbulent, and the turbulence models used are the SA one-equation model and the SST two-equation model. Spalart found that the commonly used Boussinesq vortex viscosity assumption has insufficient predictive accuracy when simulating secondary flow in pipe flow because it does not consider the anisotropy of Reynolds stress. Spalart proposed a quadratic constitutive relationship (QCR) to address the deficiencies of the Boussinesq vortex viscosity assumption in turbulence simulation. The QCR method adds a nonlinear term to the linear turbulence model and can be applied to different linear turbulence models. The new definition of Reynolds stress is:

$$\tau_{ij,QCR}=\tau_{ij}-C_{r1}\left[O_{ik}\tau_{jk}+O_{jk}\tau_{ik}\right]-C_{r2}\mu_t\sqrt{2S^*_{mn}S^*_{mn}}\delta_{ij} \tag{2}$$

In which $\tau_{ij,QCR}$ represents the Reynolds stress obtained by the QCR method, τ_{ij} represents the Reynolds stress obtained based on the Boussinesq vortex viscosity assumption, μ_t represents the turbulence eddy viscosity coefficient, O_{ik} and O_{jk} represents the dimensionless rotation tensor, and S^*_{mn} represents the strain rate tensor. The specific definitions of each parameter are shown in literature [19].

3. Computational model and grid

The computational model adopts NASA's general research model CRM [5], which is a standard model released at the 6th Resistance Conference. It is a typical modern wide-body transport aircraft configuration, led by Boeing and jointly designed by NASA's subsonic fixed-wing aerodynamic technology research group and DPW organizing committee. The design Mach number is M=0.85, and the lift coefficient is $C_L = 0.5$. The model includes the wing, fuselage, tail, pod, and pylon. The article mainly focuses on two configurations, CRM-WB and CRM-WBNP, and studies their grid convergence and drag characteristics under fixed lift coefficient of $C_L = 0.5$ and average aerodynamic chord Reynolds number of $R_e = 5 \times 10^6$. The specific appearance of the two configurations is shown in Figure 1.

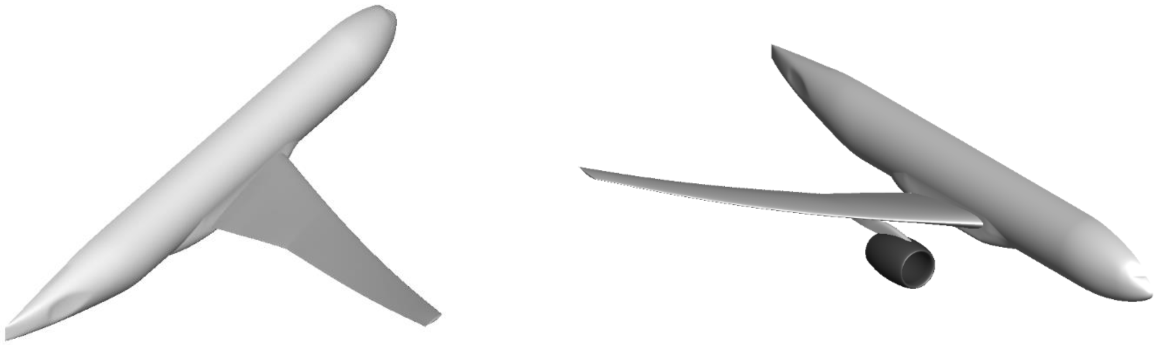

(a) CRM-WB (b) CRM-WBNP

Figure 1. CRM configuration.

CRM has conducted a series of tests in different wind tunnels, and has a large amount of detailed and reliable experimental data that can be used to verify and confirm CFD simulations. From 2010 to 2013, two phases of tests [20] were completed at the NTF (National Transonic Facility) wind tunnel at NASA Langley Research Center for different configurations, obtaining data on aerodynamic characteristics, surface pressure distribution, and model deformation. In April 2010, a comparative test [21] was conducted in the TWT (Transonic Wind Tunnel) at NASA Ames Research Center. In addition to obtaining data on the aerodynamic characteristics, surface pressure distribution, and model deformation of each configuration, pressure sensitive paint tests, friction measurement tests, and particle image velocimetry tests were also conducted. In February 2014, the German ETW (European Transonic Wind tunnel) conducted a new comparative test [22] for the CRM-WB configuration, with the same test conditions as the NTF wind tunnel. In 2012, the Japan Aerospace Exploration Agency conducted experiments in the JAXA $2m \times 2m$ transonic wind tunnel [23], and in 2016, the French Centre d'Etudes Spatiales conducted experiments in the SIMA wind tunnel [24].

The grid generation adopts a non-structural hybrid grid strategy. In order to better simulate the boundary layer flow near the object surface, triangular prism grid elements are used, while tetrahedral/pyramid fill is used in other regions. The grid spacing for the first layer is $y+ \leq 1$. A total of 4 sets of meshes were generated for the CRM-WB configuration, with a total number of mesh cells ranging from approximately 17.699 million to 61.336 million. The specific mesh information is shown in Table 1. Grid numbers are represented by grid T, grid C, grid M, and grid F, respectively.

Table 1. Number of grid cells for different grids.

Grid number	Grid T	Grid C	Grid M	Grid F
The total number of grids（million）	17.699	26.073	40.305	61.336
Number of tetrahedral meshes（million）	7.275	11.011	17.013	26.372
Number of triangular prism meshes（million）	10.379	14.997	23.204	34.842
Number of pyramid grids（million）	0.045	0.065	0.088	0.122

Figure 2 shows the grid distribution on the surface of grid C, with densification at the leading and trailing edges of the wing. The grid of CRM-WBNP is based on the grid of CRM-WB with the addition of the engine pod grid. The grid distribution is shown in Figure 3. All grids utilize parallel preprocessing techniques to quickly complete domain decomposition, and then solve the flow field through parallel computation.

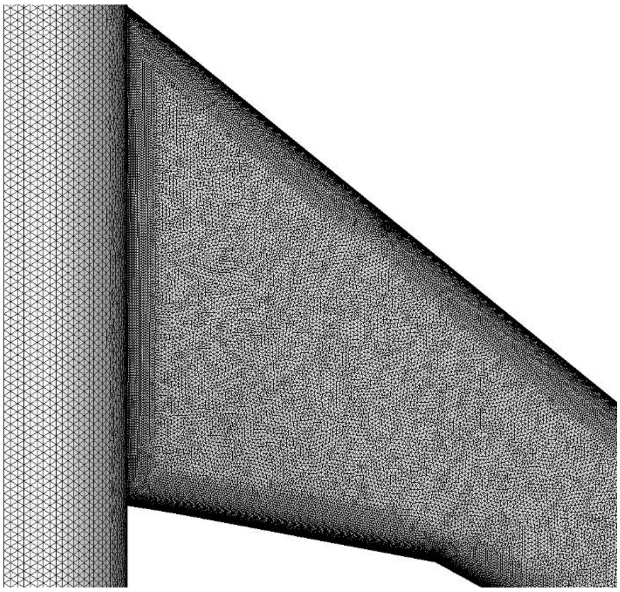

Figure 2. Surface grid of CRM-WB configuration for grid C.

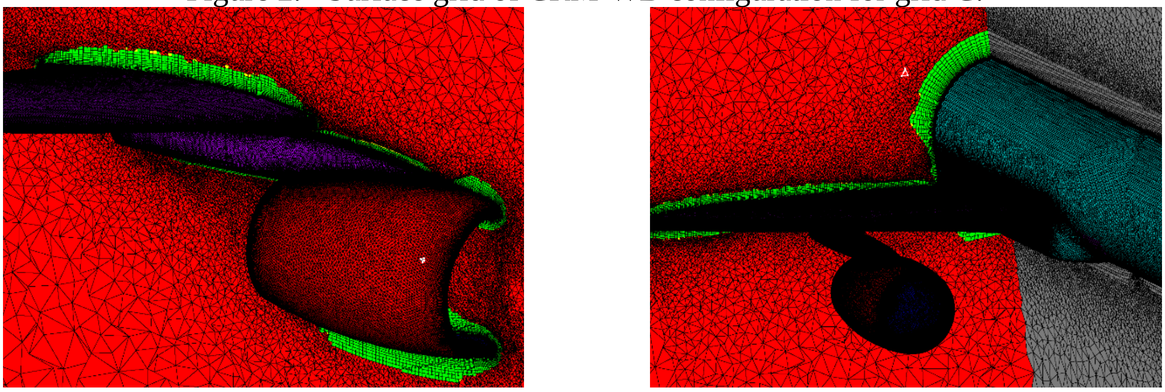

Figure 3. Grid of CRM-WBNP configuration.

4. Research on grid convergence

The quantity, distribution, and quality of the grid have a significant impact on the correctness and rationality of the numerical simulation results. Therefore, in the process of carrying out numerical simulations, it is usually first necessary to conduct grid convergence or independence studies to exclude the influence of the grid on the numerical simulation results. The main goal of grid convergence research is to estimate the grid convergence solution of forces and moments, that is, to estimate the values of forces and moments when the grid size approaches infinity. This article uses the four sets of grids described previously to conduct grid convergence studies for the CRM-WB and CRM-WBNP configurations under a fixed lift of $C_L = 0.5$.

Figure 4 shows the iteration convergence curves of lift coefficient, drag coefficient, and density residuals during the calculation in this article. The density residuals decreased by more than two orders of magnitude, and the oscillations in aerodynamic forces were within 0.2%.

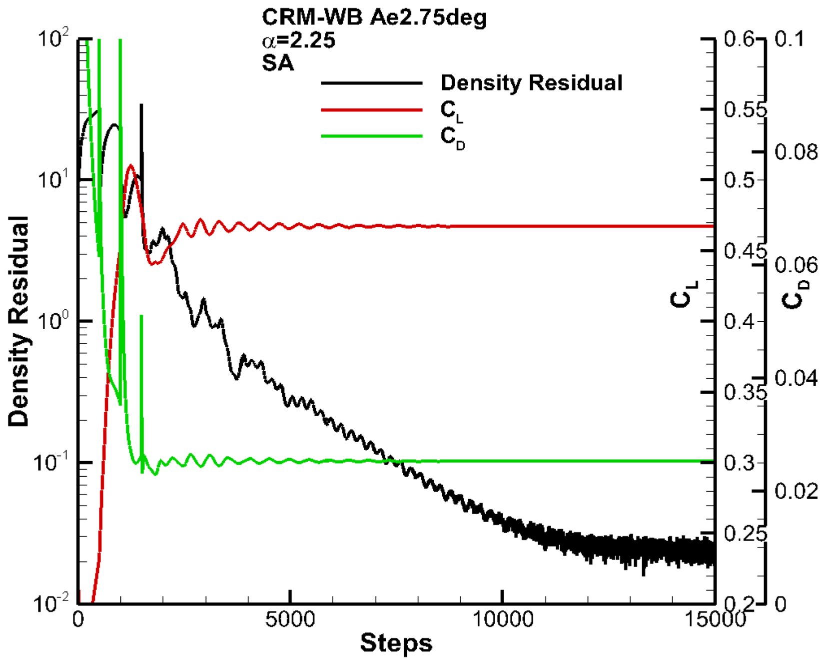

Figure 4. Convergence of force coefficient and density residual

Figure 5~Figure 9 show the grid convergence characteristics of the CRM-WBNP's external drag coefficient, pressure drag coefficient, friction drag coefficient, pitch moment coefficient, and angle of attack. The numerical method of NNW-FlowStar software is of second-order accuracy, so the abscissa is taken as $N^{-2/3}$, where N represents the number of grid cells and $N^{-2/3}$ represents the square of the characteristic scale of the grid. The grid convergence curves for drag coefficient, pressure drag coefficient, friction drag coefficient, pitching moment coefficient, and angle of attack are approximately straight lines, indicating that the spatial grid converges to second-order accuracy. When $N^{-2/3}$ is zero, it indicates that the number of grids is infinite. As can be seen from the figure, the calculated results of this article have an approximate monotonic linear convergence characteristic for the drag force and pitching moment when the grid size tends to infinity, confirming that the flow field solution is located in the asymptotic solution region, indicating that the numerical method has a convergence accuracy close to second order. As the grid is refined, the pressure difference drag coefficient (C_{DP}) decreases, while the friction drag coefficient (C_{DV}) slightly increases, leading to a decrease in the total drag coefficient (C_D). The friction resistance coefficient C_{DV} changes slightly with the grid, indicating that the boundary layer characteristics can be accurately simulated after the grid is densified to a certain extent. The calculation results of SA_QCR are consistent with those of the SA model, with only a small shift between the two methods. The total resistance obtained by SA_QCR is 1.6 counts greater than that obtained by SA, with a pressure difference resistance of 2.3 counts and a frictional resistance of approximately 0.7 counts.

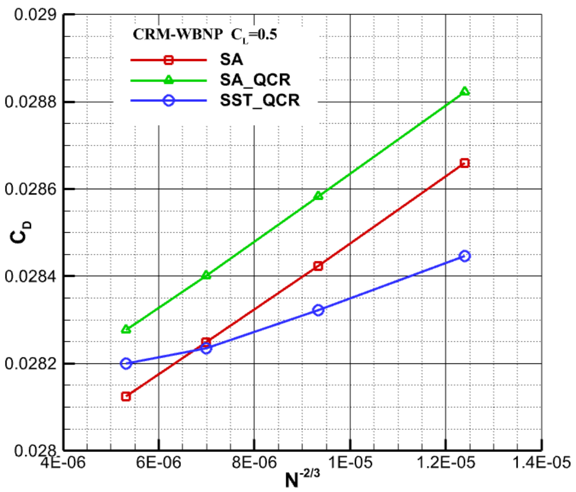

Figure 5. Grid-convergence curve of CD for CRM-WBNP.

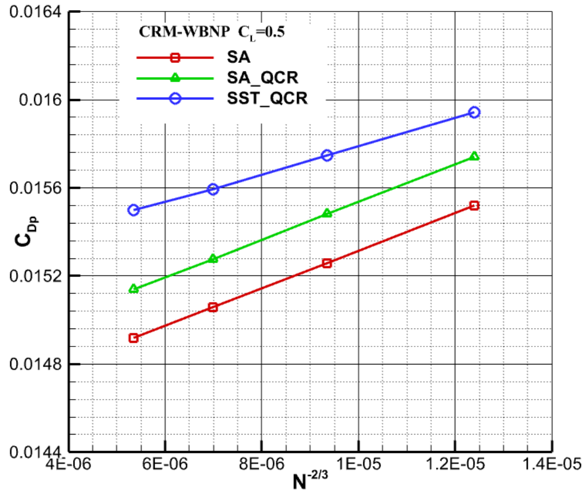

Figure 6. Grid-convergence curve of CDp for CRM-WBNP.

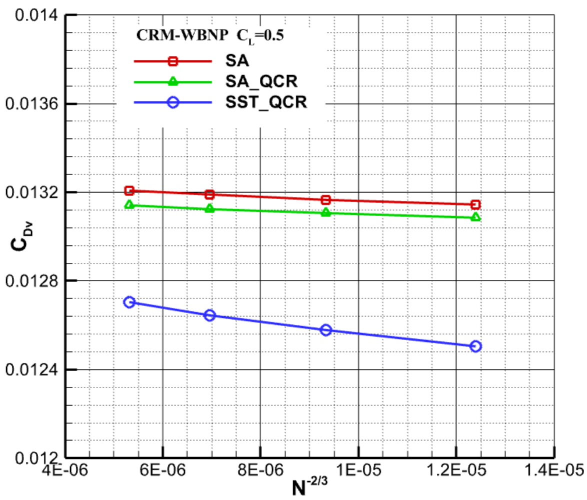

Figure 7. Grid-convergence curve of CDv for CRM-WBNP.

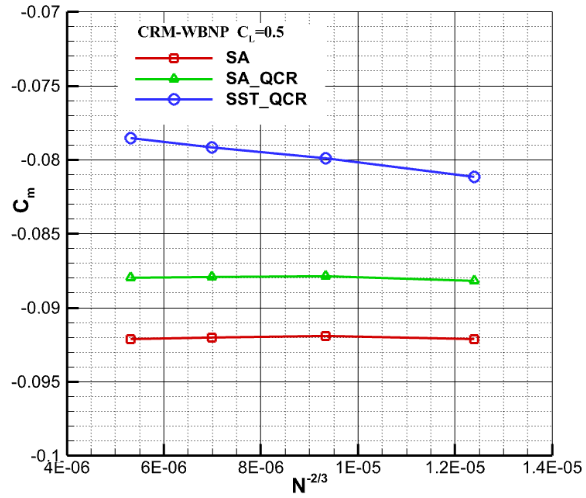

Figure 8. Grid-convergence curve of Cm for CRM-WBNP.

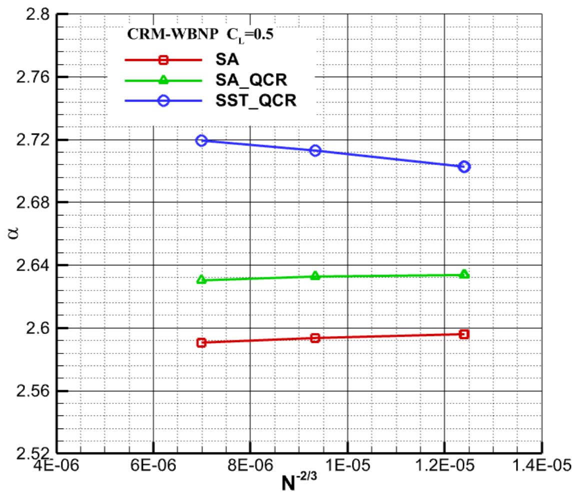

Figure 9. Grid-convergence curve of α for CRM-WBNP.

Table 2 shows the comparison of the computational results and experimental values of the CRM-WBNP shape on the dense grid grid F. The *NTF test data* represents the results of the NASA Langley Research Centre NTF wind tunnel test. The total resistance calculated by the SA, SA_QCR, and SST_QCR methods differed by less than 2 counts. When considering the drag force at a fixed lift of 0.5, the SA model is closer to the experimental value than the QCR correction, but from the perspective of the angle of attack and pitch moment at a fixed lift, the QCR method yields better results for the angle of attack and pitch moment. SST_QCR is better than SA_QCR in angle of attack and pitch moment prediction, with a larger pressure drag and a smaller friction drag, with a total drag difference within 1 count.

Table 2. Predictions with grid F for WBNP configuration

	SA	SA_QCR	SST_QCR	NTF test data
C_D (counts)	281.2	282.8	282.0	271.6
C_{Dp} (counts)	149.1	151.4	154.9	——
C_{Dv} (counts)	132.1	131.4	127.0	——
α (°)	2.588	2.629	2.725	2.941
C_m	-0.09215	-0.08797	-0.07862	-0.05284

DPW-VI focuses on the prediction accuracy of the drag increment after adding the pylon and pod. Figure 10~ Figure 12 shows the convergence characteristics of the drag increase caused by adding the pylon and pod as the grid increases, i.e., the drag increase of the CRM-WBNP configuration compared to the CRM-WB configuration as the grid increases. Table 3 compares the aerodynamic characteristic increments of the CRM-WBNP configuration, calculated using grid F, relative to the CRM-WB configuration, with experimental results. As the grid is refined, the drag increment caused by the nacelle and pylon gradually decreases, tending towards a range of 21.5 to 22.5 counts, with the increase in frictional drag contributing the majority of the drag increase. As shown in Table 3, the drag increment and angle of attack increment obtained from numerical simulation are very close to the experimental results.

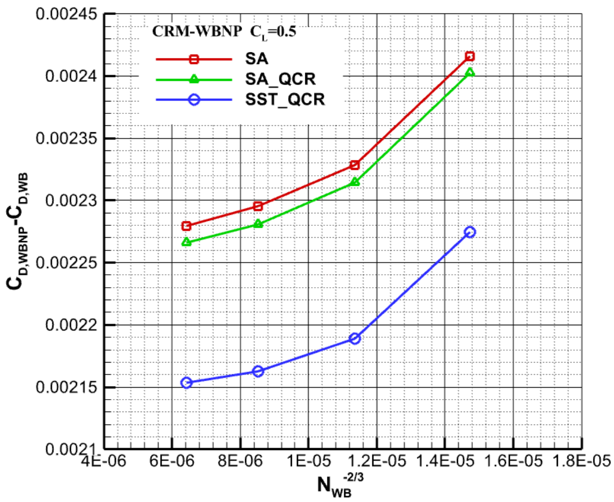

Figure 10. CD increment of CRM-WBNP compare to CRM-WB.

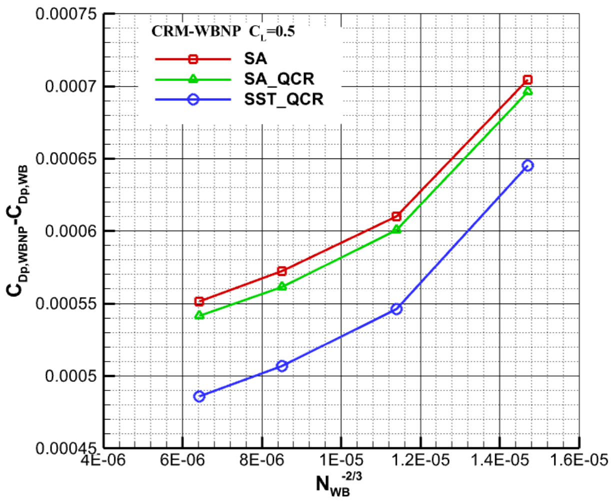

Figure 11. CDp increment of CRM-WBNP compare to CRM-WB.

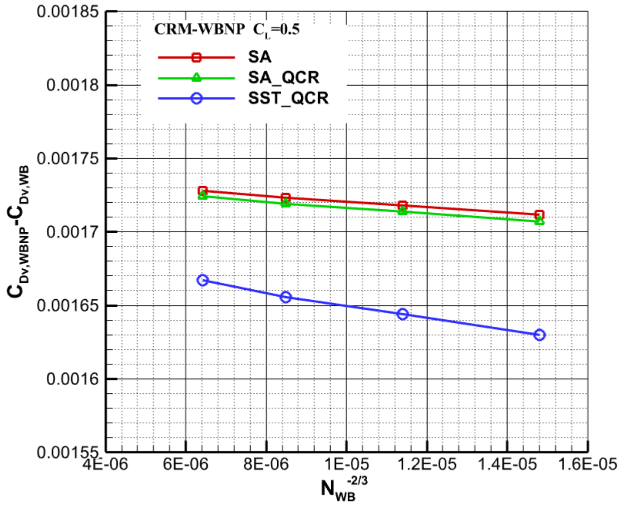

Figure 12. CDv increment of CRM-WBNP compare to CRM-WB.

Table 3. Increment predictions for CRM-WBNP compare to CRM-WB configuration with grid F

	SA	SA_QCR	SST_QCR	NTF test data
C_D (counts)	22.8	22.7	21.5	22.7
C_{Dp} (counts)	5.5	5.4	4.9	——
C_{Dv} (counts)	17.3	17.2	16.7	——
α (°)	0.158	0.159	0.159	0.150

5. Study on the influence of different turbulence models

To further verify the ability of NNW-FlowStar software to simulate transport aircraft, a comparative analysis and study was conducted based on the CRM-WB shape and the effects of four turbulence models: SA, SST, SA_QCR, and SST_QCR. Figure 13~ Figure 15 shows the lift, drag, and pitching moment characteristics calculated by different turbulence models compared with experimental values. *AMES test data* and *NTF test data* represent the test results of the AMES wind tunnel and NTF wind tunnel, respectively. As can be seen from Figure 13, the variation of lift coefficient for the original SA and SST models is consistent. At an angle of attack of 3.5°, there is a significant advance flow separation, resulting in stall, a decrease in lift coefficient, and an obvious inflection point in the lift curve. As the angle of attack increases further, the lift coefficient begins to climb again, and before the angle of attack approaches 4°, the lift line bends for the second time, and the slope of the lift line decreases. After using the QCR method, the prediction accuracy of lift characteristics was significantly improved, and the phenomenon of flow separation ahead of time at an angle of attack of 3.5° disappeared. Compared with experimental values, there was a small difference in the variation of lift coefficient with angle of attack. The lift coefficient of SA_QCR was about 0.03~0.04 different from the experimental value, and the lift coefficient of SST_QCR was about 0.01~0.03 different from the experimental value. From the resistance characteristic curves and pitch moment characteristic curves in Figures 14 and 15, it can be seen that the calculation results obtained using the QCR method are in better agreement with the test results. Figure 16 shows the comparison of surface streamlines and wing separation bubbles at an angle of attack of 3.5°. The flow separation in the near-wall region is typically characterized by the component of the surface friction coefficient in the streamwise direction, C_{fx}. The blue region in the figure indicates the location where $C_{fx} < 0$, indicating the presence of separation.

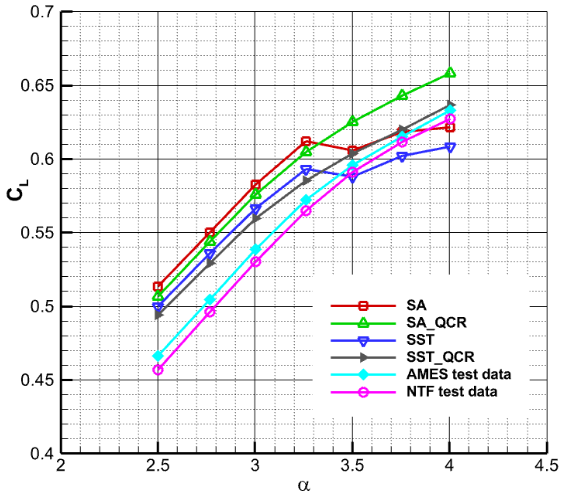

Figure 13. Lift predictions for CRM-WB configuration.

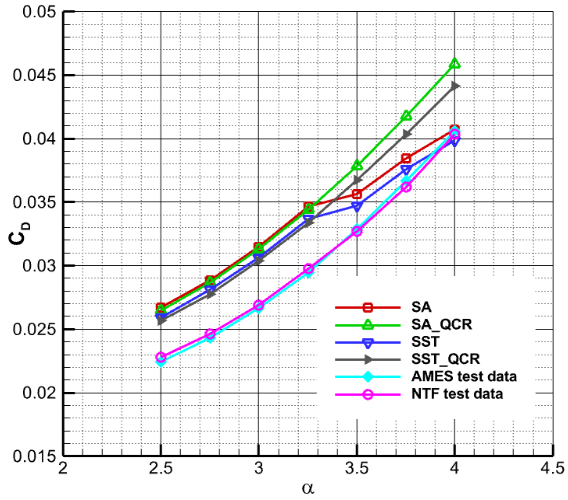

Figure 14. Drag predictions for CRM-WB configuration.

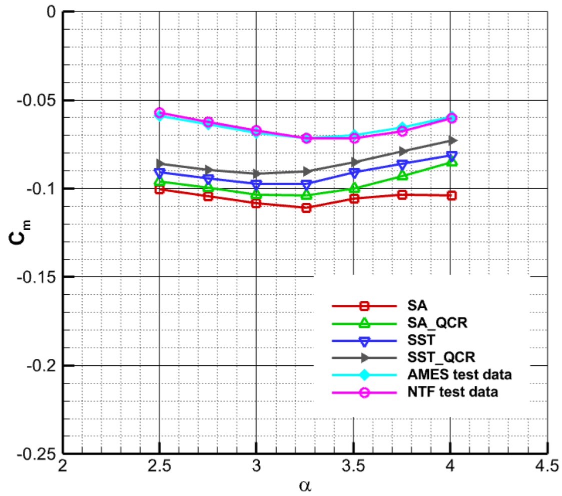

Figure 15. Pitching moment predictions for CRM-WB configuration.

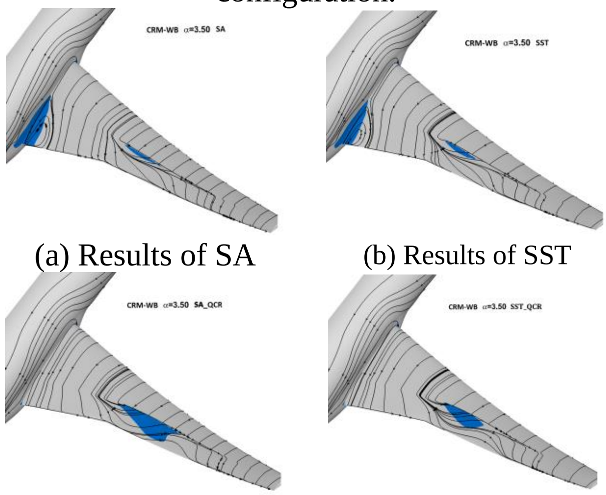

(a) Results of SA (b) Results of SST

(c) Results of SA_QC (d) Results of SST_QC

Figure 16. Comparison of surface streamlines and separation bubble.

Figure 17 shows the pressure distribution comparison at spanwise locations of 0.131 and 0.502 at an angle of attack of 3.5°. It can be seen that the original SA or SST model exhibits large separation bubbles at the wing-body junction, resulting in a forward shift and weakening of the shock wave at η=0.131, and a significant reduction in lift. When using the QCR method, no separation bubbles appear at the junction of the wing and body, but there is a large separation behind the wave in the middle of the wing, resulting in a significant shock wave moving forward at η=0.502 and a loss of lift. This further validates the variation pattern of the lift characteristic curve in Figure 13. In summary, it can be seen that using the QCR method, the calculated results are in better agreement with experimental values, especially at larger angles of attack, avoiding premature separation at the wing root. The SST_QCR method has the best agreement with experimental values, validating the ability of the method to simulate the flow field of transport aircrafts.

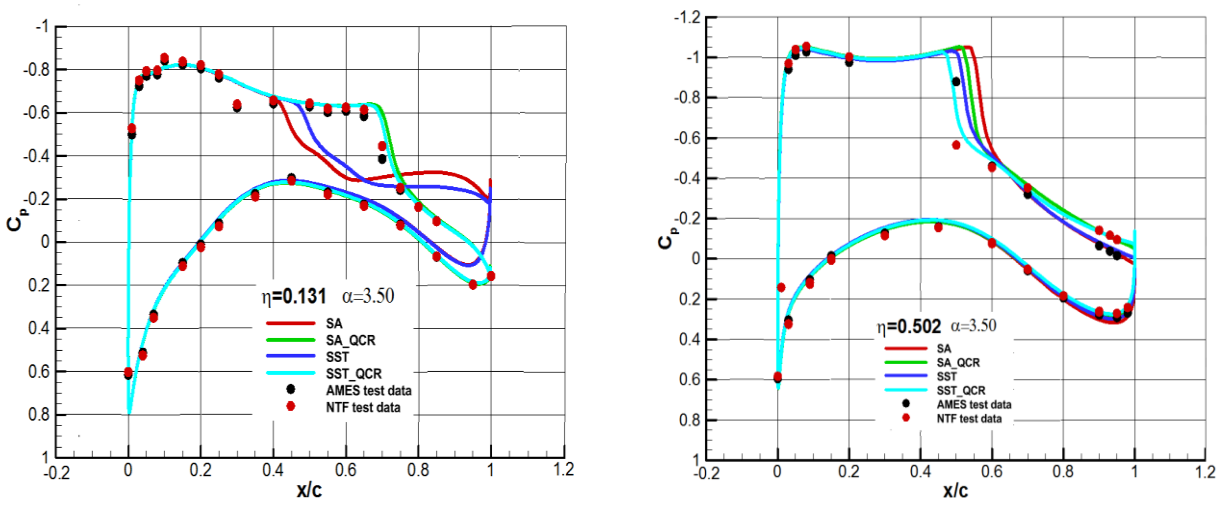

(a) Spanwise locations of η =0.131 (a) Spanwise locations of η =0.502

Figure 17. Comparison of Cp prediction with experimental data.

6. Conclusion

Based on the CRM benchmark, the NNW-FlowStar software was used to simulate the transport aircraft. The effects of grid convergence, different turbulence models, and secondary constitutive corrections were investigated. The prediction accuracy of drag increment after adding pylon and pod was analyzed.

1) The grid convergence characteristics of the approximate linearity are calculated, indicating that the numerical method in this article has second-order accuracy.

2) The QCR correction method can effectively avoid the early separation of the wing root during the calculation of the CRM benchmark model, resulting in better agreement between the aerodynamic characteristics and pressure distribution obtained and the experimental values.

3) The flow field separation vortex structure and pressure distribution obtained by the SST turbulence model with QCR correction method are in best agreement with the experimental results, confirming the reliability of the method for simulating the flow of transport aircraft.

Acknowledgments

This work was financially supported by National Numerical Windtunnel fund.

References

[1] SLOTNICK J, KHODADOUST A, ALONSO J, et al. CFD vision 2030 study: a path to revolutionary aerosciences. NASA/CR-2014 -218178[R]. Washington, D. C. : NASA, 2014.

[2] JAMESON A. Re-engineering the design process through computation[J]. Journal of Aircraft, 1999, 36(1): 36-50.

[3] GOLDHAMMER M I. Boeing 787 – design for optimal airplane performance[C]. CEAS/KATnet Conference on Key Aerodynamic Technologies, Bremen, Germany, June 2005.

[4] LI Shang-bin, LIN Yong-feng, FAN Feng.The Research of aerodynamic characteristics of tilt rotor using wind tunnel test and numerical simulation methods[J]. ENGINEERING MECHANICS, 2018,35(6): 249-256(in Chinese).

[5] EDWARD N. T., OLAF P B, STEFAN K., et al. Summary of data from the sixth AIAA CFD drag prediction workshop: CRM cases 2 to 5: AIAA-2017 -1208[R]. Grapevine, Texas: AIAA, 2017.

[6] DEBONIS J., RUMSEY C., MALIK M. Test cases for NASA's revolutionary computational aerosciences technical challenge[C]// AIAA SciTech 2015, Kissimmee, FL: NF1676L-20545.

[7] LEVY D. W., ZICKUHR T., VASSBERG J. C., et al. Summary of data from the first AIAA CFD drag predication workshop, AIAA-2002-0811[R]. Reston: AIAA, 2002.

[8] WANG Y. T. An overview of DPW IV ~ DPW VI numerical simulation technology[J]. Acta Aeronautica et Astronautica Sinica, 2018, 39(4): 021836 (in Chinese).

[9] LAFLIN K. R., KLAUSMEYER S. M., ZICKUHR T., et al. Summary of data from the second AIAA computational fluid dynamics drag predication workshop[J]. Journal of Aircraft, 2005,42(5): 1165-1178.

[10] VASSBERG J. C., TINOCO E. N., MANI M., et al. Abridged summary of the third AIAA CFD drag predication workshop[J]. Journal of Aircraft, 2008,45(3): 781-798.

[11] JOHN C. V., EDWARD N. T., MORI M., et al. Summary of the fourth AIAA computational fluid dynamics drag prediction workshop[J], Journal of Aircraft, 2014, 51(4): 1070-1089.

[12] DAVID W. L., KELLY R L., EDWARD N. T., et al. Summary of data from the fifth computational fluid dynamics drag prediction workshop[J], Journal of Aircraft, 2014, 51(4): 1194-1213.

[13] DENG X. G., ZONG W. G., ZHANG L. P., et al. Verification and validation in computational fluid dynamics[J]. Advances in Mechanics, 2007, 37(2): 279-288 (in Chinese).

[14] CHEN S. S., LIU L. Y., YAN C., et al. Design and realization of automated testing cloud platform for CFD verification and validation[J]. Acta Aeronautica et Astronautica Sinica, 2017, 38(3): 12909 (in Chinese).

[15] LI Q., LIU D. W., XU X., et al. Experimental study of aerodynamic characteristics of CHN-T1 standard model in 2.4m transonic wind tunnel[J]. Acta Aerodynamica SInica, 2019, 37(2): 337-342(in Chinese).

[16] ZHAO W., CHEN J. T., XIAO W., Advances in the key technologies of verification and validation system of National Numerical Windtunnel project[J]. Acta Aerodynamica SInica, 2020,38(6): 1165-1172 (in Chinese).

[17] CHEN J. Q., WU X. J., ZHANG J., et al. FlowStar: General unstructured-grid CFD software for National Numerical Windtunnel (NNW) Project[J]. Acta Aeronautica et Astronautica Sinica, 2021, 42(9):625739 (in Chinese).

[18] ZHANG J, ZHOU NC, LI M, et al. R & D and design of industrial CFD software for Aeronautics and Astronautics[J]. Journal of Software, 2022 33(5): 1529-1550.

[19] MANI M., BABCOCK D. A., WINKLER C. M., et al. Predictions of a supersonic turbulence flow in a square duct: AIAA-2013 -0860[R]. Grapevine, Texas. : AIAA, 2013.

[20] RIVERS M. B., DITTBEMER A. Experimental investigation of the NASA common research model: AIAA-2010-4218[R]. Reston, VA: AIAA, 2010.

[21] RIVERS M. B., DITTBEMER A. Experimental investigation of the NASA common research model in the NASA Langley transonic facility and NASA Ames 11-ft transonic wind tunnel: AIAA-2011-1126[R]. Reston, VA: AIAA, 2011.

[22] RIVERS M. B., RUDNIK R., QUEST J. Comparison of the NASA common research model European transonic wind tunnel test data to NASA test data: AIAA-2015-1093[R]. Reston, VA: AIAA, 2015.

[23] UENO M., KOHZAI T., KOGA S., et al. 80% scaled NASA common research model wind tunnel test of JAXA at relatively low Reynolds number: AIAA-2013-0493[R]. Reston, VA: AIAA, 2013.

[24] CARTIERI A., HUE D., CHANZY Q., et al. Experimental investigations on the common research model at ONERA-SIMA -Comparison with DPW numerical results: AIAA-2017-0964[R]. Reston, VA: AIAA, 2017.

[25] ZHANG J, LIU J, ZHOU N, et al. ParTransgrid: A scalable parallel preprocessing tool for unstructured-grid cell-centered computational fluid dynamics applications[J]. Software Pract Exper. 2023, 53(1):6-26.